Theme Article: Art and Cultural Heritage

A Classification Method of Oracle Materials Based on Local Convolutional Neural Network Framework

Shanxiong Chen
Southwest University

Han Xu
Southwest University

Gao Weizhe
Southwest University

Liu Xuxin
Southwest University

Mo Bofeng
Capital Normal University

***Abstract*—The classification of materials of oracle bone is one of the most basic aspects for oracle bone morphology. However, the classification method depending on experts' experience requires long-term learning and accumulation for professional knowledge. This article presents a multiregional convolutional neural network to classify the rubbings of oracle bones. First, we detected the "shield grain" and "tooth grain" on the oracle bone rubbings, then complete the division of multiple areas on an image of oracle bone. Second, the convolutional neural network is used to extract the features of each region and we complete the fusion of multiple local features. Finally, the classification of tortoise shell and animal bone was realized. Utilizing the image of oracle bone provided by experts, we conducted an experiment; the result show our method has better classification accuracy. It has made contributions to the progress of the study of oracle bone morphology.**

Digital Object Identifier 10.1109/MCG.2020.2973109
Date of publication 20 February 2020; date of current version 28 April 2020.

Oracle inscriptions are inscribed on tortoise shells and animal bones in the Shang Dynasty. To study oracle inscriptions, we should not only pay

Published by the IEEE Computer Society

attention to the inscription itself, but also attach importance to the information, such as materials and forms that the text is attached to. Dong Zuobin, Bing Zhi, and Zeng Yigong and many other famous oracle experts implemented the research on oracle materials and forms. Professor Huang Tianshu, an expert on oracle inscription, even proposed to establish a branch of "oracle morphology" [1] so as to study specially the materials and forms of oracle bones. Therefore, the research on this aspect has its unique value. The research on oracle morphology can include many aspects, such as material, shape, location, drilling shape, and the split shape of Bu Zhao, among which, the most important issue is the material of oracle bone. In the past, some important books of oracle inscription, such as *The Collection of Oracle Bone Inscriptions*,[2] *Supplement to the Collection of Oracle Bone Inscriptions*,[3] etc., did not contain the information of materials. However, newly published books, such as *The Collection of Oracle Bones in the Institute of History, Chinese Academy of Social Sciences,*[4] *The Collection of Oracle Bones in Lushun Museum,*[5] and *The Collection of Oracle Bones in Fudan University,*[6] all fully marked the information of materials after checking the original oracle pieces, which shows that the academia is more and more aware of the unique role of material in the study of oracle bones. Although some books have labeled the information of oracle bone materials, most of the oracle inscription literature published in the past do not have the information, so there are still a large number of oracle materials to be classified. From the actual publication situation for oracle bone material, this classification work can only rely on the rubbing images of oracle. Generally, the classification of oracle materials based on oracle rubbings is based on the experience of experts in the field of oracle science, while becoming an expert requires long-term learning and accumulation. In this article, based on the study of traditional classification of oracle materials by expert experience, convolutional neural network (CNN) was used to classify oracle rubbings automatically. Through scanning and imaging the oracle bone rubbings, we used feature extraction and classification prediction of CNN framework, established the material classification and recognition model of oracle bone rubbings and realized the automatic identification of tortoise shell and animal bone rubbings, which is a preliminary attempt in artificial intelligence technology to assist the identification of oracle morphology.

IMAGE CLASSIFICATION MODEL BASED ON CNN

Image classification can use artificial intelligence technology, especially machine learning methods, to enable computers to recognize and classify images, which plays an important role in the field of pattern recognition. At present, image classification methods are mainly divided into two categories:[7] classification based on image space and classification based on feature space. The classification based on image space mainly uses the underlying features of image such as color, gray, texture, shape, and position to classify the image.[8,9] Classification based on feature space realizes image classification by mapping the original image to high-dimensional space and extracting its high-level features, which can effectively reduce the dimensionality of data and the complexity of computing process.[10] Therefore, the classification results largely depend on the adaptability of feature extraction methods.

In recent years, in the field of image classification, more in-depth learning methods are used to extract features. In particular, since 2006, Professor Hinton has proposed that the training difficulty of in-depth neural network can be greatly reduced by layer-by-layer initialization method, which effectively solves the problem of large-scale learning in in-depth training.[11] Since then, the architecture of CNN has developed rapidly and achieved good application results in different fields. This is a meaningful work that AlexNet framework[12] is proposed by Alex Krizhevsky in 2012 (as shown in Figure 1). In the Alexnet, ReLu, Dropout and LRN are used for CNN for the first time, the GPU is used to improve the computing speed. Alexnet has a deeper network level than LeNet. From Level 5 of LeNet to Level 7 of AlexNet, AlexNet won the first place in the ImageNet competition that year. AlexNet not only has more and deeper layers of neural networks than LeNet, it also can learn more complex high-dimensional features of images. With AlexNet's success, researchers have proposed other ways to improve it. The most famous ones are ZFNet,[13] VGGNet,[14] GoogleNet,[15] and ResNet.[16,17] In terms of framework, the trend of

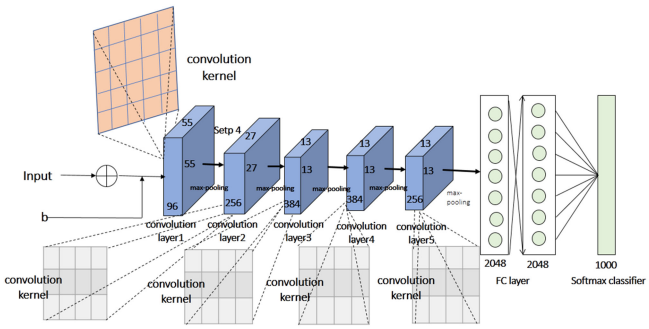

Figure 1. Simplified AlexNet framework.

CNN development is the increasing number of layers. ResNet,[18] the champion of ILSVRC 2015, is more than 20 times as much as AlexNet and eight times as much as VGGNet. By increasing the depth, the network can use the increased nonlinearity to obtain the approximate framework of the objective function and get better characterization.

The framework of convolutional neural network completes data analysis and processing by constructing a complex model framework. One of its important applications is image classification and recognition, so it is also very suitable for oracle image classification. For a long time, the classification of oracle inscriptions puci has relied on expert observation, completely relying on the experience and knowledge of experts in the field. The introduction of neural network classification and recognition technology and the exploration of automatic machine classification cannot only solidify the knowledge of experts in the field into computer models, but also facilitate the analysis of existing classification systems and methods, and further promote the development of oracle bone classification. In this article, the classification of oracle bone rubbings is studied by extracting the features of oracle bone rubbings, the transformation from the original image to the feature space is realized, and the automatic classification of oracle bone rubbings is completed in the feature space.

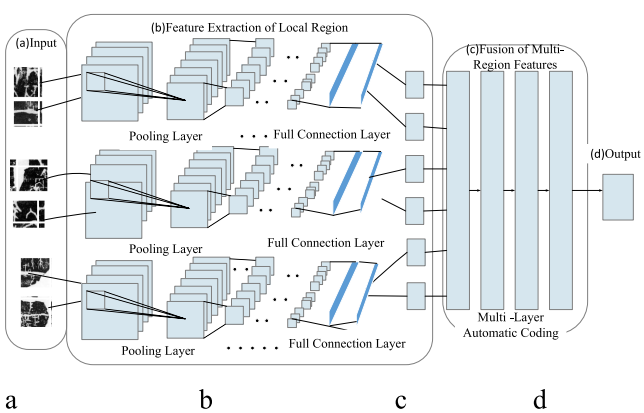

Figure 2. Classification framework of oracle bone rubbings based on local CNN.

CLASSIFICATION MODEL OF ORACLE BONE RUBBINGS BASED ON LOCAL CNN

The task of this article is to implement the automatic classification of tortoise shell and animal bone in oracle rubbings. The classification of tortoise shells and animal bones by oracle experts is mainly based on the "shield grain" and "tooth grain" on the oracle rubbings. Because only the tortoise shells can have these two characteristic. However, since the oracle bones have gone through thousands of years, the erosion often lead to many natural cracks on the oracle bones, which are easily confused with "shield grain" and "tooth grain" in rubbings. In addition, it is difficult to use mathematical models to define the description of "shield grain" and "tooth grain" by oracle bone experts. In this article, we use the local feature of oracle bone rubbings to improve the performance of oracle bone rubbings classification. Combining with the hierarchical feature extraction of CNN,[19] we propose to use the framework of local convolution neural network to classify oracle bone rubbings automatically. The framework of the model can be seen in Figure 2. It consists of four parts, specifically as follows.

(a) The data input of the model, which consists of three local regions, namely "shield grain" region, "tooth grain" region, and "nonshield grain and nontooth grain" region. (b) Each region corresponds to a feature extraction subnet. Each subnet consists of two Conv-Pooling-ReLU layers and two fully connected layers. These subnets extract the function of each local region. (c) Multifeature fusion subnet, which consists of four Autoencoding (AE) layers,[20] through which, fusion features can be obtained. (d) The output of the model. The Softmax layer is used to predict the type of input data. In order to extract the features of local region, the rules of local region partition of oracle bone rubbings are provided.

Division of Local Region of Oracle Bone Rubbings

In this article, the oracle bone rubbings are classified and recognized by multiregion local feature extraction. The key is to divide the region of oracle bone rubbings. Because the biggest feature difference between tortoise shell and animal bone is "shield grain" and "tooth grain" (as shown in Figure 3), it is necessary to retain the information of "shield grain" and "tooth grain" when dividing image region, especially if the image is just segmented from "shield grain," which destroys the feature information of image and is not conducive to classification. According to the observation of the image, it can be found that the gradient of the pixels at the "shield grain" varies greatly, and the "tooth grain" lies on the edge of the image and is not smooth and its derivative is discontinuous. We divide the image into regions according to the order from top to bottom and from left to right. The principles are as follows.

1) The regions with large gradient variation are not segmented and merged into one region with the upper part of the image to avoid segmenting the "shield grain" region.
2) Take the derivative of each pixel on the edge of the curve, and the edge regions with discontinuous derivatives are not segmented to avoid segmenting the "tooth grain" region.
3) Considering that the local features are more conducive to the classification of oracle bones, when dividing the regions in horizontal and vertical directions, the principle of zoning is "more should be followed," that is, the direction with a large number of regional divisions should be chosen.

(1) Regional division of "shield grain."

In this article, Laplace operator is used to detect the shield grain region,[21] and finish the division of image region. Assuming that $f(x, y)$ is an oracle bone image, since Laplace operator is isotropic, then there is

$$\nabla f(x,y) = \frac{\partial^2 f(x,y)}{x^2} + \frac{\partial^2 f(x,y)}{y^2} + \ldots. \tag{1}$$

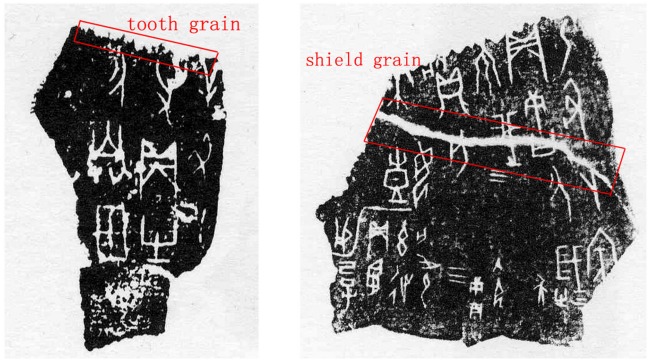

Figure 3. Characteristics of "tooth grain " and "shield grain." (a) Tooth grain. (b) Shield grain.

Laplace operator is the divergence of gradient

$$\begin{aligned} \Delta f &= \nabla \cdot \nabla f \\ \Delta \triangleq \nabla^2 \triangleq \nabla \cdot \nabla &= \left(\frac{\partial f}{\partial x}\vec{i} + \frac{\partial f}{\partial y}\vec{j}\right) \cdot \left(\frac{\partial f}{\partial x}\vec{i} + \frac{\partial f}{\partial y}\vec{j}\right) \\ &= \frac{\partial^2 f}{\partial x^2} + \frac{\partial^2 f}{\partial y^2}. \end{aligned} \tag{2}$$

Since the image is a discrete two-dimensional matrix, the differential is approximated by the difference.

$$\begin{aligned} \frac{\partial^2 f}{\partial x^2} &= \frac{\partial G_x}{\partial x} = \frac{\partial [f(i,j) - f(i,j-1)]}{\partial x} \\ &= \frac{\partial f(i,j)}{\partial x} - \frac{\partial f(i,j-1)}{\partial x} \\ &= [f(i,j+1) - f(i,j)] - [f(i,j) - f(i,j-1)] \\ &= f(i,j+1) - 2f(i,j) + f(i,j-1) \\ \frac{\partial^2 f}{\partial x^2} &= f(i+1,j) - 2f(i,j) + f(i-1,j). \end{aligned} \tag{3}$$

Therefore,

$$\begin{aligned} \Delta f = {} & f(x+1,y) + f(x-1,y) + f(x,y+1) \\ & + f(x,y-1) - 4f(x,y). \end{aligned} \tag{4}$$

Laplace operator is used to detect the edge of the shield grain area of the oracle bone rubbings (as shown in Figure 4). It can be seen that the oracle rubbing are divided into connected regions. By calculating the area and aspect ratio of each connected region, shield marks can be effectively divided, thus providing a basis for the segmentation of the later oracle rubbings.

The discriminant method of shield grain area is as follows.

1) Let Q_i represent an initial connected region selected after binaryzation oracle images have been carry out edge detection by Laplace operator. When the search is conducted in four directions around Q_i with variable Δ, the connected domain Q_i correspondingly becomes $Q_{i+\Delta}$. If searching hit an edge, searching in this direction is stopped, otherwise, $Q_i = Q_{i+\Delta}$, continue to searching.
2) The area ratio of area Q_i to the rubbings area was calculated, $q(i) = |S|/|Q_i|$, S is the area of oracle bones rubbings, further, calculated the aspect ratio of the region, $w(i)$. when $q(i) > w(i)$, area Q_i is the shield grain.

The algorithm is described as follows.

Algorithm 1.

Input: Binary image of Oracle Bone rubbings I, Δ is a variable.
Output: the area of shield grain, M

```
I = Laplace(I)// Using Laplace to detect edge of Image I
Select an initial connected region Qi in I.
    if Qi + Δ1 is not the edge of the curve, then Qi1 = Qi + Δ1, else this direction search is terminated //Δ1 is the increment to the left of region Qi
    if Qi + Δ2 is not the edge of the curve, then Qi2 = Qi + Δ2, else this direction search is terminated //Δ2 is the increment to the top of region Qi
    if Qi + Δ3 is not the edge of the curve, then Qi3 = Qi + Δ3, else this direction search is terminated //Δ3 is the increment to the right of region Qi
    if Qi + Δ4 is not the edge of the curve, then Qi4 = Qi + Δ4, else this direction search is terminated //Δ4 is the increment to the bottom of region Qi
calculating q(i) = |S|/|Qi|, w(i)
if q(i) > w(i) then M(i) = q(i)
End
```

(2) Regional detection of "tooth grain."

For the detection of "tooth grain" on oracle bone rubbings, we introduce arc differential to calculate the curvature of each point on the edge of oracle bone, and further judge the variation of curvature per unit length so as to determine whether or not it is a tooth grain.

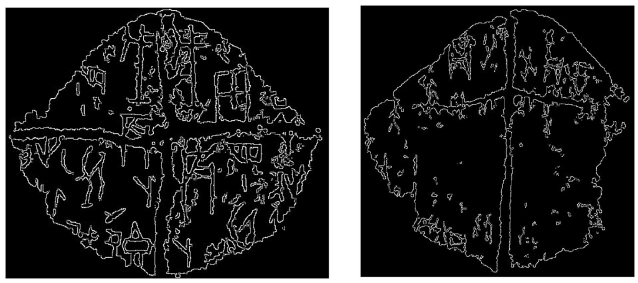

Figure 4. Edge detection of shield grain.

Let C be the edge curve of oracle bone, and its equation is $r = r(s)$, wherein, s is the arc length parameter of the curve, and $r'(s)$ is the unit tangent vector field of Curve C. Assuming

$$\alpha(s) = r'(s). \tag{5}$$

Here, $\alpha(s)$ is the direction vector of Curve C at s, so when a point moves along the curve at a unit rate, the rotation speed of the direction vector reflects the curvature of the edge curve. Here, the rotation speed of the direction vector $\alpha(s)$is measured by $|\alpha'(s)|$. Since $\alpha(s)$ is a unit tangent vector field of Curve $r = r(s)$, the angle between Vector $\alpha(s + \Delta s)$ and $\alpha(s)$ is expressed by $\Delta\theta$, then $\lim_{\Delta s \to 0} |\Delta\theta/\Delta s| = |\alpha(s)|$.

Let $k = |a'(s)|$, then K is the curvature of Curve $r = r(s)$ at s, and $a'(s)$ is the curvature vector of the curve. The unit tangent vector $a'(s)$ of Curve C is moved parallel to the origin, and the tangent parametric equation of the curve is as follows:

$$r = \alpha(s). \tag{6}$$

Generally, s is an arc length parameter of tangent. The arc length element of tangent is expressed as $d\tilde{s} = |\alpha'(s)|ds = kds$. So, the curvature of oracle bone edge curve at s can be expressed as$k = d\tilde{s}/ds$. Since the rate of curvature variation is the basis for judging the tooth grain, the second derivative of the oracle bone edge curve is used to judge the tooth grain region, that is $\eta = d^2\tilde{s}/ds^2$. By calculating the η value on the edge curve of oracle bones and combining with the decision threshold value, the region of tooth grain can be divided.

The algorithm is described as follows.

Algorithm 2.

Input: Binary image of Oracle Bone rubbings I, threshold ε

Output: the area of tooth grain X

I = Laplace(I) // Using Laplace to detect edge of Image I

Selecting any curve on the edge, C

For $i = 1$ to len(C)

Calculating $\alpha(s) = r'(s)$ //$\alpha(s)$ is the unit tangent vector at the point s. s belongs to C.

Calculating $k = |\alpha'(s)|$//k is the curvature of the curve C at point s.

$d\tilde{s} = |\alpha'(s)|ds = kds$

$k = d\tilde{s}/ds$

$\eta = d^2\tilde{s}/ds^2$ //$\boldsymbol{\eta}$ is curvature change rate of oracle bone edge curve

If $\eta > \varepsilon$, $X(i) = s$

End for circulation

If len(X)>len(C)/3, X is the area of tooth grain

End

Regional Feature Extraction Based on CNN

In order to obtain effective features, we use CNN as feature extractor for each region. Generally, CNN consists of multiple convolution processes and fully connected processes. For each convolution process, it consists of four parts: convolution layer, local response normalization layer, nonlinear transformation layer and convergence layer (as shown in Figure 5). Here, we choose a region containing a "shield grain" as an example to describe the convolution process. $I^{m\times n\times c}$ is the input of CNN, where each dimension represents the width, height, and channel of the image. The convolution layer calculates the convolution kernel W of the input image and filter and increases the offset B as

$$R = W \otimes I + b \tag{7}$$

wherein $\otimes$ represents convolution operation, $R^{m'\times n'\times c'}$ is the output. The activation function ReLU is used in the nonlinear transformation layer as

$$\tilde{R} = \max\{0, R\}. \tag{8}$$

For the normalized layer of local response of the oracle bone rubbing image,[11] after applying ReLU, it becomes as follows:

$$\hat{R}^i_{x,y} = \tilde{R}^i_{x,y} \Big/ \left(k + \alpha \sum_{j=\max(0,i-n/2)}^{\min(N-1,i+n/2)} \left(\tilde{R}^i_{x,y}\right)^2 \right)^{\beta} \tag{9}$$

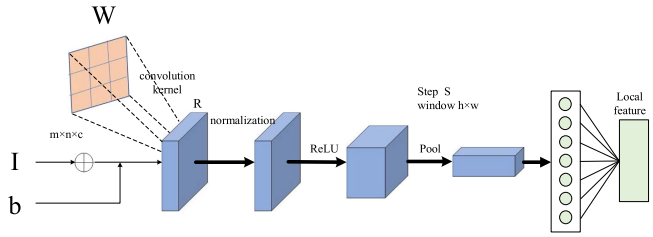

Figure 5. CNN-based region feature extraction framework.

where $\tilde{R}^i_{x,y}$ represents the network layer activation calculated by the convolution kernel at x and y after applying ReLU. $\hat{R}^i_{x,y}$ represents the normalized activation of local response. In this article, a normalization method called BatchNorm was used to optimize the training parameters. This method improves the training speed and speeds up the convergence (it essentially smooths the loss surface, making it easier to find the global optimum during training). This method can avoid overfitting, simplify the parameter adjustment process, and fit the network structure of CNN. N represents the number of kernels. k, n, $\boldsymbol{\alpha}$, and $\boldsymbol{\beta}$ are hyperparameters. Therefore, the $\hat{R}$ is downsampled by using the maximum pooling layer as

$$\bar{R} = \max_{h\times w,s}\{\hat{R}\}. \tag{10}$$

Among them, $h \times w$ is a subwindow and s is the step length of sliding window. The whole fully connected layer is constructed by CNN, so the CNN feature extraction of local region is expressed as follows:

$$F = \Phi(I, \theta). \tag{11}$$

Φ represents the connection process of full convolution. I is the input information. θ includes the filter convolution kernel W and offset B.

Multiple Local Feature Fusion

Through the above steps, we get the features of each local region. Since the features of each local region are composed of vectors, we use the AE[20,22] network to fuse these features and reduce the region size.

Assuming that image I contains N regions $O_i, i \in \{1, 2, \ldots, N\}$, at the same time, each object region O_i contains M pixels. For each pixel $I_j, j \in \{1, 2, \ldots, M\}$ in object O_i, the feature of each pixel is $\boldsymbol{f}_j$, and the feature of each region is

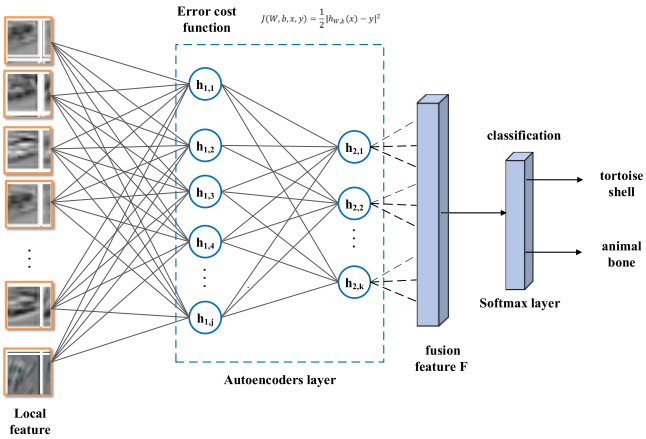

Figure 6. Feature fusion structure of Multilocal area.

r_j. We construct a block $U_j = [f_j, r_j]$ of depth feature of the image in each region for feature classification of the original image at the pixel level. The label of region O_i is mainly determined by vector U_j statistics as

$$P_j = W_2 \tanh\left(W_1 W U_j + b_1\right) \tag{12}$$

$$d_{i,a} = \frac{1}{t(O_i)} \sum_{j \in [1,M]} \text{count}\left(P_j = a\right). \tag{13}$$

Matrixes W_1 and W_2 are the training parameters of CNN classifier, P_j is the prediction label, $t(O_i)$ is the number of pixels of the object, and the characteristics of the final object O_i are as follows:

$$F_i = \text{argmax}\ d_{i,a}. \tag{14}$$

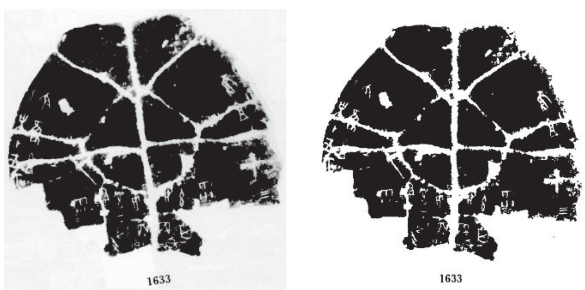

(a) (b)

Figure 7. Effects before and after Oracle image processing. (a) Raw oracle bone image. (b) Image of oracle bone after denoising, correction and enhancement. The pictures are the oracle bone rubbing of numbered 1633 from. The Collection of Oracle Bone Inscriptions (chief editor Guo Moruo, editor-in-chief Hu Houxuan, Published by Zhonghua Bookstore from 1978 to 1983; used with permission).

The whole fusion process is shown in Figure 6.

(1) First, these feature vectors are cascaded with other feature vectors as global feature vectors $Q = [q_0, q_1, q_2 \ldots q_n]$. Q is the input to the autocoded network.
(2) A hierarchical automatic coding network is established to fuse these features and reduce the feature dimension. Q is inputted into the network whose output is the final fusion feature F.
(3) Finally, the Softmax layer is used to identify the categories after merging the regions.

EXPERIMENTS AND ANALYSIS

The dataset contains 1476 rubbings of tortoise shell and 300 rubbings of ox bone. We choose one-third as the test set and two-thirds as the training set, the 5-fold cross-validation method is adopted. The oracle bone rubbings in the dataset are provided by the Oracle Research Center of Capital Normal University. They are derived from the illustration of related research works and the scanned images of oracle bone rubbings. Because the original image size is different, the image quality is uneven, and there is noise in the images.

After analysis and testing, we used nonlocal mean filtering to process the image, eliminate the noise, enhance the image contrast through Gamma correction, and adjust the size of all images to 500 × 500 pixels. Taking into account the different angles of the various oracle bones in the process of imaging, we corrected all the oracle bone rubbings so that the oracle bones were located in the middle of the image (as shown in Figure 7).

The task of this section is to divide the oracle bone images into regions according to the method in the section titled "Classification Model of Oracle Bone," and then conduct training in the framework of CNN to extract regional features and establish the classification model of oracle bone rubbings. Finally, after implementing region segmentation to rubbings that type is unknown, the classification of the images of oracle bones was completed by using the trained CNN framework. Experimental environment: CPU Intel(R) core(7M) i7-7700 Ghz; Memory DDR4, 8.00 G;GPU NVIDA

GeForce RTX 2080 SUPER, basic frequency 1650 MHz, acceleration frequency 1815 MHz, video memory: GDDR6, 8 G, 256 bit, video memory frequency 15.5 Ghz, video memory bandwidth 496 GB/s.

(1) A comparison between the classification of integral oracle bone rubbings and the classification of local regions.

The division of oracle bones follows the Rules (1) and (2), that is, no "shield grain" and "tooth grain" are segmented. Considering the efficiency of image processing, this article divides the region vertically and horizontally (as shown in Figure 8), scans the oracle bone images from top to bottom and from left to right so as to complete the region segmentation. In order to verify the influence of segmentation direction on classification impact, we divide the training data in horizontal and vertical directions, and put the segmentation region into the CNN framework for training. Then, we divide the test data into horizontal and vertical directions, respectively, and send them into the trained model for classification.

In the experiment, we selected the horizontal and vertical directions to test, respectively. Two thirds is the training set and one third is the test set. In order to verify the influence of cutting direction on classification accuracy, we conducted cross-validation in two directions. The experiment adopted LeNet, AlexNet, GoogleNet, Vgg19Net, DenseNe, and ResNet for CNN frameworks. In order to test the best batch size, we set the batch size to 8,64,72,128, respectively, and compared the Loss value through multiple tests .we found that batch 64 is optimal. For the optimization part of the framework, we use Adam stochastic gradient descent optimization algorithm for training. During training, it is necessary to set the learning rate to control the update speed of parameters. This parameter will greatly affect the model convergence speed. If learning rate is too small, it will be slow convergence, increase the training cost. If learning rate is too big, it will cause the parameter to oscillate near the optimal solution, so the optimal solution cannot be obtained. The experiment analyzed the variation of loss value under the condition of multiple learning rates. When the number of training is 2000, the learning rate is 0.2, 0.02, and

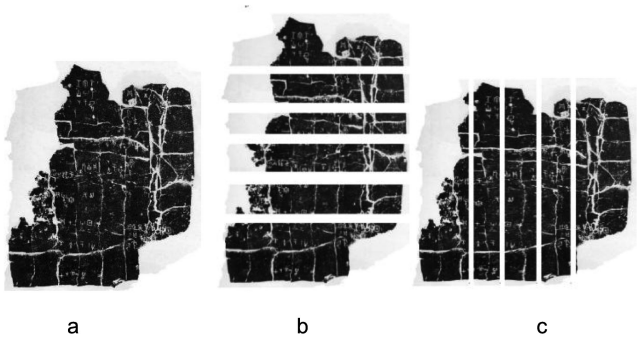

Figure 8. Horizontal and vertical regional division. (a) Original image. (b) Horizontal segmentation. (c) Vertical segmentation. The pictures are the oracle bone rubbing of numbered 1140 (a), horizontal segmentation (b), and vertical segmentation (c) from The Collection of Oracle Bone Inscriptions (chief editor Guo Moruo, editor-in-chief Hu Houxuan, Published by Zhonghua Bookstore from 1978 to 1983; used with permission).

0.002, respectively, the curve of discriminator loss function is shown in Figure 9. The horizontal axis represents the training times, and the vertical axis represents loss.

From Figure 9, it is obviously that the loss value starts to shake violently after 1240 times, when the learning rate is 0.2. This is because the learning rate is too high, it cannot converge on the best point. Comparing the loss values of learning rate 0.002 and learning rate 0.02. The loss value of the learning rate 0.002 is closer to 1, so the prediction value would be closer to 1. In this article, the experiment is carried out again on the basis of learning rate 0.02. When the training times are 2000, the discriminator loss function curve is shown in Figure 10 for the learning rate 0.09, 0.002, and 0.001. From Figure 10, it can be determined that when the learning rate is 0.09, the loss value

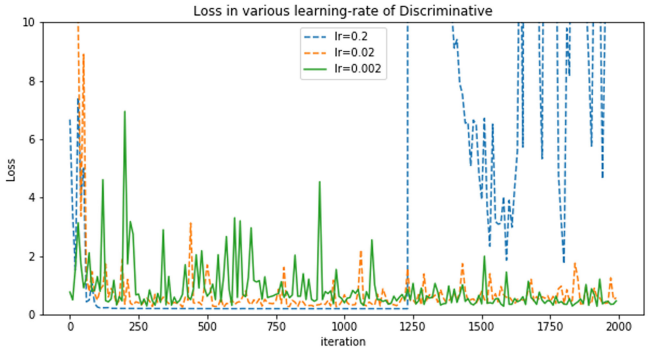

Figure 9. Change curve of the loss values of the learning rates 0.2, 0.02, and 0.002.

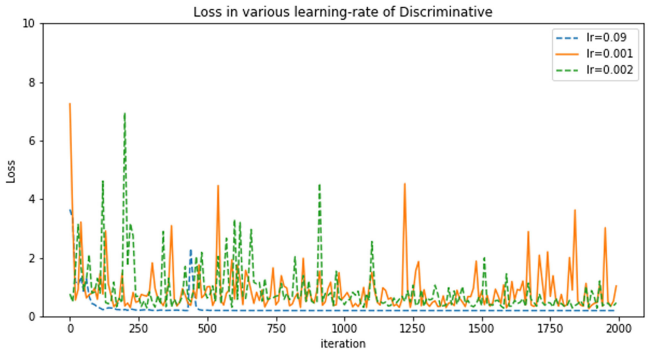

Figure 10. Change curve of loss values for learning rates of 0.09, 0.002, and 0.003.

is closest to 1. Therefore, the learning rate is set as 0.09 in this article, and the same parameters are used in subsequent experiments.

After determining the parameters, we tested the effect of segmentation direction on classification. It can be seen from Table 1 that the classification accuracy (ACC) after segmenting region is significantly higher than unsegmenting. Alexnet's has good classification accuracy for Oracle rubbings. The area segmentation in horizontal direction is more accurate than that in vertical direction. Further observation shows that the accuracy of training and test set in the same direction segmentation is higher than that in different directions. It also shows that the consistency of data has a certain impact on the classification accuracy.

(2) The impact of the segmented number of local regions on the classification accuracy.

In order to further quantify the impact of regional segmentation on the classification accuracy of oracle bone rubbings, we studied the relationship between the number of different regions segmented on different oracle bone rubbings and the classification accuracy. In the experiment, all the oracle bone rubbings in the dataset were segmented in horizontal and vertical directions to ensure that the "tooth grain" and "shield grain" were not segmented. The oracle bone rubbings are classified according to the number of segmented regions, and the relationship between the number of regions and classification accuracy is analyzed, as shown in Table 2.

According to the distribution of "shield grain" of oracle bone rubbings, each image is segmented vertically and horizontally, and the images with the most segmented regions are selected as samples. After the region segmentation of the image is completed, we select the oracle bone rubbings that contain one region, two regions, three regions, four regions, and five or more regions.

The size of each oracle bone rubbings is 500 × 500. After segmentation, the size of each area is inconsistent. To facilitate processing, we rearrange the image of each area from top to bottom, from left to right, to 100 × 100. The insufficient part is filled with white. Then LeNet, AlexNet, GoogleNet, Vgg19Net, DenseNe, and ResNet are used to train and identify. The experimental results show that the classification effect of oracle bone rubbings is the best when the image is divided into three or four regions. This is because too few regions cannot achieve the expression of local features, leading to the method of local features CNN proposed in this article cannot fuse each region very well. With the increase of segmented regions,

Table 1. Classification accuracy of vertical and horizontal segmentation.

	Training set (horizontal segmentation)		Training set (vertical segmentation)		Nonregional segmentation
Model name	Test set (horizontal segmentation)	Test set (vertical Segmentation)	Test set (horizontal segmentation)	Test set (vertical segmentation)	
LeNet [11]	0.785	0.773	0.775	0.787	0.715
AlexNet [12]	**0.843**	0.781	0.801	**0.839**	**0.753**
GoogleNet [15]	0.774	0.759	0.761	0.773	0.728
Vgg19Net [23]	0.805	0.763	0.775	0.793	0.681
DenseNet [24]	0.817	0.805	0.792	0.801	0.729
ResNet [16]	0.787	0.775	0.763	0.782	0.704

CNN can extract and fuse the features of each region more accurately. Therefore, our method has good classification accuracy. When the image has five or more regions, too many regions make the oracle bone rubbings more fragmented, and it has a better expression for the characteristics of the single region, while the overall feature distortion of the oracle bone rubbings is larger, so the classification accuracy is reduced. At the same time, it can also be seen in Table 2 that the more areas are divided, the time required for the network increases correspondingly, and the FPS (Frames Per Second) value increases gradually with the increase of the number of areas. This is because more partitions increase the time of network training and recognition, thus affect the performance of the whole network.

(3) The impact of the number of detected tooth grain on classification.

In the section titled "Division of local region of oracle bone rubbings," the second derivative of the oracle bone edge curve is given and used to judge the tooth grain region, i.e., $\eta = d^2\tilde{s}/ds^2$. Therefore, the η value on the edge curve of oracle bone can be calculated, and the tooth grain region can be divided by combining with the decision threshold. Here we analyze the impact of the number of detected teeth grain on the classification of oracle bones. First, we scanned the edge of oracle bone rubbings according to the method in the section titled "Division of local region of oracle bone rubbings," and drew the edge curve. Then, we calculate η value according to the points of the edge curve, and through setting threshold, the points that reach and exceed the upper limit of the threshold are aggregated into the teeth grains. Finally, we traversed the whole edge curve and got the number of teeth grains.

As shown in Figure 11, the abscissa represents the threshold, the ordinate represents the number of tooth grains, and the step length of threshold setting interval (0.1–0.8) is 0.5. The ηv value is calculated through the edge curve of each oracle bone rubbings in the training set and the test set, the number of tooth grains in the training set and the test set is obtained by the 5-fold cross method. It can be seen that with the increase of the threshold, the number of tooth grains is gradually rising,

Table 2. Classification accuracy of different numbers of segmented local regions.

Model Name \ Number of regions	1	2	3	4	5 or above
LeNet[10]	0.736	0.785	**0.817**	**0.811**	0.803
AlexNet[11]	0.782	0.813	**0.836**	**0.837**	0.792
GoogleNet[14]	0.714	0.808	**0.814**	**0.803**	0.783
Vgg19Net[22]	0.739	0.786	**0.819**	**0.826**	0.815
DenseNet[23]	0.724	0.779	**0.823**	**0.831**	0.822
ResNet[15]	0.732	0.794	**0.835**	**0.841**	0.837

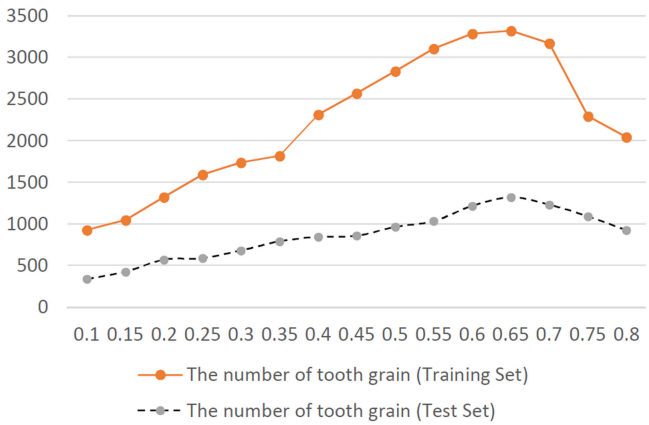

Figure 11. Impact of threshold on the number of teeth grain.

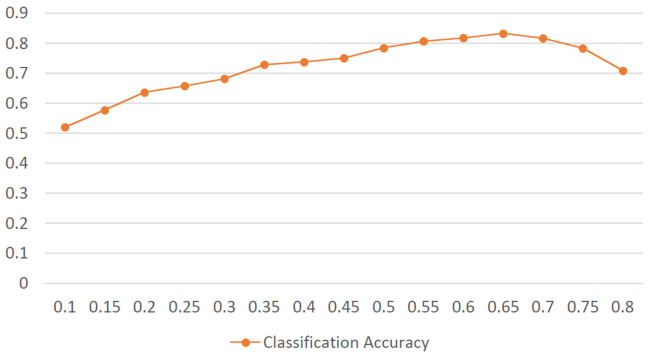

Figure 12. Impact of threshold on classification accuracy.

reaching the maximum at the threshold of 0.65, and the impact of the number of tooth grains on the classification accuracy is synchronous. Figure 12 shows the results of training and classification by using AlexNet network.

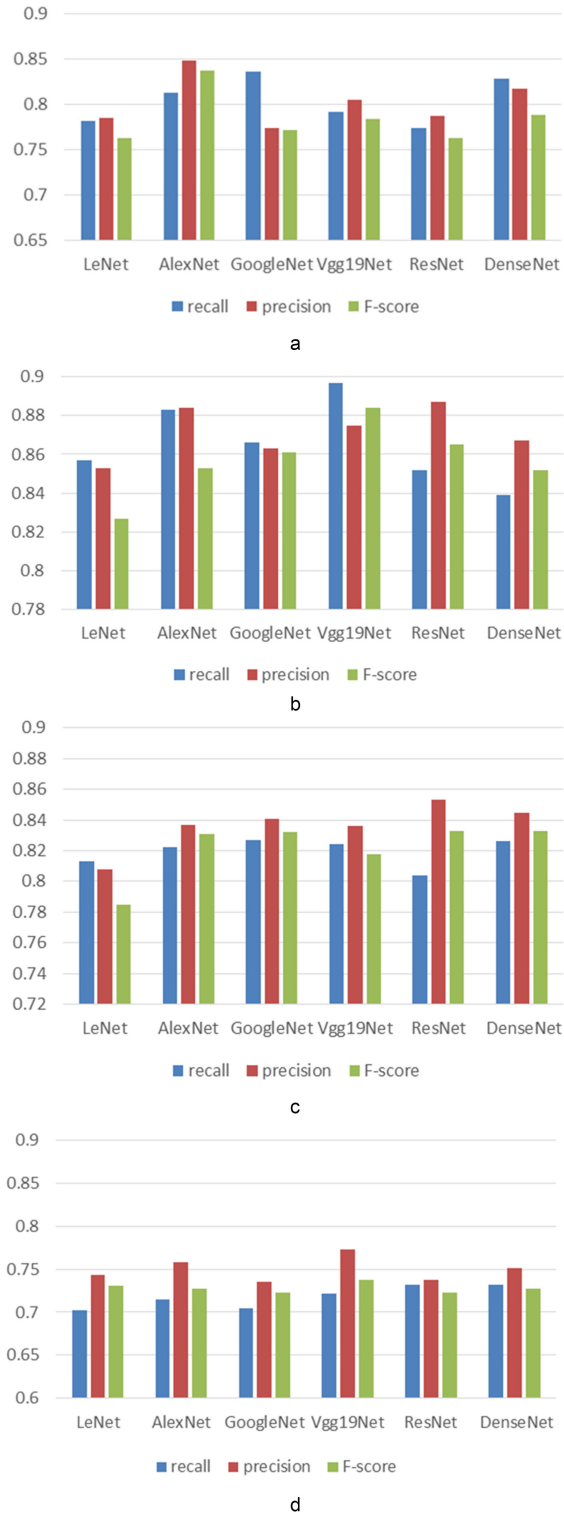

Figure 13. Recall, precision, and F-score after classification by using LeNet, AlexNet, GoogleNet, Vgg19Net, DenseNet, and ResNet in four cases. (a) Unlabeled+ divided region. (b) Labeled+ divided region. (c) Labeled + undivided region. (d) Unlabeled + undivided region.

The abscissa represents the threshold and the ordinate represents the classification accuracy. The results are consistent with those in Figure 6. The optimal classification accuracy is achieved near the threshold of 0.65.

(4) The impact of labeling on the characteristics of "tooth grain" and "shield grain" on classification.

The important feature of distinguishing tortoise shells from animal bones in oracle bone rubbings is the "teeth grain" and "shield grain" on oracle bones. In this article, two kinds of features are labeled to train CNN network. We selected two-thirds of the images and invited the experts of Oracle Research Center of Capital Normal University to label them as training set and one-third as test set. It can be seen from Figure 13 that Recall, Precision, and F-score have been improved to different degrees after using the method of region division, which not only labels but also divides the regions, so that the classification effect is the best. Recall, Precision, and F-score of vgg19net have reached 0.897, 0.875, and 0.884, respectively, which are close to the artificial classification results of oracle bone experts. (Because the oracle bone rubbings themselves are part of the oracle bone fragments, after thousands of years, some fragments are worn seriously. The classification accuracy of oracle bone experts in this dataset is 0.92.)

CONCLUSION

The use of artificial intelligence technology to classify the material of oracle bone rubbings is a basic subject in the study of oracle bone morphology, which will play an exemplary and guiding role in other related research, and provide an auxiliary role for the study of oracle bone conjugation and oracle bone font classification. In this article, a convolution neural network method based on local region division is proposed to classify oracle bone rubbings. Through the detection of "shield grain" and "tooth grain" on oracle bone rubbings, the division of multiple regions on the image of oracle bone is completed. The features are extracted and further fused by CNN; finally, the classification of tortoise shells and animal bones is realized. The

experimental results show that the method proposed in this article is close to the classification effect of related experts, but considering the serious wear of some oracle bone rubbings, future work will study how to enhance the edge of oracle bone rubbings and enhance the feature expression of the region.

ACKNOWLEDGMENTS

This work was supported in part by the National Social Science Fund of China under Grant 19BYY171, in part by the Open Projects Program of National Laboratory of Pattern Recognition, China Postdoctoral Science Foundation under Grant 2015M580765, in part by the Chongqing Postdoctoral Science Foundation under Grant Xm2016041, in part by the Fundamental Research Funds for the Central Universities, China under Grant XDJK2018B020, in part by the Chongqing Natural Science Foundation under Grant cstc2019jcyj-msxmX0130, and in part by the Chongqing City Science and Technology Education Research Projects under Grant KJQN201801901.

REFERENCES

1. T. S. Hang, *A Collection of Bones and Tortoise Shells*. Cambridge, MA, USA: Academic, 2010, Art. no. 515.
2. M. R. Guo and H. X. Hu, *The Collection of Oracle Bone Inscriptions*. Beijing, China: Zhong Hua Book Company, pp. 1978–1983, 1999.
3. J. B. Peng, J. Xie, and J. F. Ma, *Supplement to the Collection of Oracle Bone Inscription*. Beijing: Language Press, 1999, pp. 895–907.
4. Z. H. Song, P. Zhao, and J. F. Ma, *The Collection of Oracle Bones in the Institute of History*. Shanghai: Chinese Academy of Social Sciences, Shanghai Ancient Books Publishing Press, 2014, pp. 457–462.
5. Z. H. Song and F. C. Guo, *The Collection of Oracle Bones in Lushun Museum*. Shanghai: Shanghai Ancient Books Publishing Press, 2014, pp. 239–314.
6. J. Lu and L. Ge, *The Collection of Bones and Tortoise Shell of Fudan University*. Shanghai: Shanghai Ancient Books Publishing Press, Fudan University Press, 2019, pp. 578–591.
7. Y. L Tian *et al.*, "Review on image scene classification technology," *Acta Electron. Sinica*, vol. 47, no. 4, pp. 915–926, 2019.
8. K. Q Huang, W. Q Ren, and T. N Tan, "A review on image object classification and detection," *Chin. J. Comput.*, vol. 37, no. 6, pp. 1225–1240, 2014.
9. J. Bi J and C. S. Zhang, "An empirical comparison on state-of-the-art multi-class imbalance learning algorithms and a new diversified ensemble learning scheme," *Knowl.-Based Syst.*, vol. 158, pp. 81–93, 2018.
10. I., Murtza, A. Khan, and N. Akhtar, "Object detection using hybridization of static and dynamic feature spaces and its exploitation by ensemble classification," *Neural Comput. Appl.*, vol. 31, no. 2, pp. 347–361, 2019.
11. G. E. Hinton, S. Osindero, and Y. W. Teh, "A fast learning algorithm for deep belief nets," *Neural Comput.*, vol. 18, no. 7, pp. 1527–1554, 2006.
12. A. Krizhevsky, I. Sutskever, and G.E. Hinton, "ImageNet classification with deep convolutional neural networks," in *Proc. Conf. Workshop Neural Inf. Process. Syst.*, 2012, pp. 1097–1105.
13. M. D. Zeiler and R. Fergus, Visualizing and understanding convolutional networks. in *Proc. Eur. Conf. Comput. Vis.*, 2014, vol. 8689, pp. 818–833.
14. K. Simonyan and A. Zisserman, "Very deep convolutional networks for large-scale image recognition," computer science. in *Proc. Int. Conf. Learn. Representations*, 2015, pp. 1304–1317.
15. C. Szegedy *et al.*, "Going deeper with convolutions," in *Proc. IEEE Conf. Comput. Vis. Pattern Recognit.*, 2015, pp. 1–9.
16. K. He *et al.*, "Deep residual learning for image recognition," in *Proc. IEEE Conf. Comput. Vis. Pattern Recognit.*, 2016, pp. 770–778.
17. K. He, X. Zhang, S. Ren, and J. Sun, "*Identity mappings in deep residual networks*," in *Proc. Eur. Conf. Comput. Vis.*, 2016, vol. 9908, pp. 630–645.
18. K. He *et al.*, "*Deep residual learning for image recognition*," in *Proc. IEEE Conf. Comput. Vision Pattern Recognit. IEEE Comput. Soc.*, 2016, pp. 770–778.
19. W. Zhao *et al.*, "Superpixel-based multiple local CNN for panchromatic and multispectral image classification," *IEEE Trans. Geosci. Remote Sens.*, vol. 55, no. 7, pp. 4141–4156, Jul. 2017.
20. E. P. Ijjina and C. K. Mohan, "Classification of human actions using pose-based features and stacked auto encoder," *Pattern Recognit. Lett.*, vol. 83, pp. 268–277, 2016.
21. M. S. Fraczek, "The hyperbolic Laplace-Beltrami operator," *Selberg Zeta Functions Transfer Operators: Exp. Approach Singular Perturbations*. vol. 2139, pp. 87–127, 2017.

22. R. X. Wang and D. C. Tao, "Non-local auto-encoder with collaborative stabilization for image restoration," *IEEE Trans. Image Process.*, vol. 25, no. 5, pp. 2117–2129, May 2016.
23. I. Hammad and K. El-Sankary, "Impact of approximate multipliers on VGG deep learning network," *IEEE Access*, vol. 6, pp. 60438–60444, 2018.
24. G. Huang *et al.*, "Densely connected convolutional networks," in *Proc. IEEE Conf. Comput. Vis. Pattern Recognit.*, 2017, pp. 4700–4708.

Shanxiong Chen was a visiting scholar with South Australia University in 2014. He is currently an Associate Professor with the College of Computer and Information Science, Southwest University, China. He currently holds a postdoctoral position with Southwest University. His research interests include machine learning, pattern recognition, and data mining. He received the Ph.D. degree in computer science and technology from the College of Computer, ChongQing University. He is the corresponding author of this article. Contact him at csxpml@163.com.

Han Xu is currently working toward the master's degree in software engineering with Southwest University, Chongqing, China. His research interests include deep learning and image processing. He received the bachelor's degree in software engineering from the Taiyuan University of Technology in 2017. Contact him at 544600530@qq.com.

Gao Weize is currently working toward the master's degree in computer technology with Southwest University, Chongqing, China. His research interests include pattern recognition and image processing. He received the bachelor's degree in computer science and technology from the Guizhou University of Engineering Science in 2019. Contact him at 1309719643@qq.com.

Liu Xuxing is currently working toward the master's degree in software engineering with Southwest University, Chongqing, China. His research interests include deep learning and image processing. He received the bachelor's degree in plant protection from SouthWest University in 2019. Contact him at lxx249@163.com.

Bofeng Mo is currently an Associate Research Fellow with the Center for Oracle Bone Studies, Capital Normal University, Beijing, China. His research interests include Chinese Paleography and Chinese classical philology. He received the Ph.D. degree in literature from the School of Literature, Capital Normal University. Contact him at mbf2001@163.com.